CSIRO PUBLISHING

International Journal of Wildland Fire **2017**, *26*, 755–771
https://doi.org/10.1071/WF17019

Indicators of burn severity at extended temporal scales: a decade of ecosystem response in mixed-conifer forests of western Montana

Sarah A. Lewis[A,D], *Andrew T. Hudak*[A], *Peter R. Robichaud*[A], *Penelope Morgan*[B], *Kevin L. Satterberg*[B], *Eva K. Strand*[B], *Alistair M. S. Smith*[B], *Joseph A. Zamudio*[C] *and Leigh B. Lentile*[B]

[A]USDA, Forest Service, Rocky Mountain Research Station, 1221 South Main Street, Moscow, ID 83843, USA.
[B]Department of Forest, Rangeland, and Fire Sciences, University of Idaho, 975 West 6th Street, Moscow, ID 83844, USA.
[C]Unmanned Aircraft Systems USA (UASUSA), 229 Airport Road, East Hangar, Longmont, CO 80503, USA.
[D]Corresponding author. Email: sarahlewis@fs.fed.us

Abstract. We collected field and remotely sensed data spanning 10 years after three 2003 Montana wildfires to monitor ecological change across multiple temporal and spatial scales. Multiple endmember spectral mixture analysis was used to create post-fire maps of: char, soil, green (GV) and non-photosynthetic (NPV) vegetation from high-resolution 2003 hyperspectral (HS) and 2007 QuickBird (QB) imagery, and from Landsat 5 and 8 imagery collected on anniversary dates in 2002, 2003 (post fire), 2004, 2007 and 2013. Initial estimates of char and NPV from the HS images were significantly correlated with their ground-measured counterparts ($\rho = 0.60$ ($P = 0.03$) and 0.68 ($P = 0.01$) respectively), whereas HS GV and Landsat GV were correlated with canopy GV ($\rho = 0.75$ and 0.70 ($P = 0.003$) respectively). HS imagery had stronger direct correlations with all classes of fine-scale ground data than Landsat and also had stronger predictive correlations with 10-year canopy data ($\rho = 0.65$ ($P = 0.02$) to 0.84 ($P = 0.0003$)). There was less than 5% understorey GV cover on the sites initially, but by 2013, it had increased to nearly 60% regardless of initial condition. The data suggest it took twice as long for understorey GV and NPV to replace char and soil as primary ground cover components on the high-burn-severity sites compared with other sites.

Additional keywords: char, hyperspectral remote sensing, multiple endmember spectral mixture analysis, QuickBird.

Received 17 February 2016, accepted 12 June 2017, published online 6 September 2017

Introduction

The potential of wildland fires to influence the cycle of carbon dynamics and ecosystem composition is widely recognised (Dale *et al.* 2001; Loehman *et al.* 2014; Rocca *et al.* 2014). Remote sensing is the most suitable method for monitoring these fire effects over extended spatial and temporal scales (Lentile *et al.* 2006; Morgan *et al.* 2014). Characterising severity and ecological condition of the post-fire environment (e.g. distance to seed source, vegetation structure and composition, likelihood of soil erosion) is important for forecasting future effects on ecological systems (Lentile *et al.* 2006; Hayes and Robeson 2011). The majority of severity assessments focus on either the immediate post-fire changes or effects in the year following the fire, especially when severity products from the Monitoring Trends in Burn Severity (MTBS) project are utilised (Cocke *et al.* 2005; Lentile *et al.* 2006, 2009; Kolden *et al.* 2015). Studies employing MTBS products are also spectrally and spatially constrained; spectrally, they only employ two spectral indices that have been widely critiqued (Roy *et al.* 2006; Kolden *et al.* 2015; Smith *et al.* 2016), while spatially, they are limited to data at the scale of Landsat pixels (30 m). In contrast, the post-fire environment is heterogeneous, with considerable spatial variability even within comparable burned patches at the scale of a Landsat pixel (Smith *et al.* 2005) that may or may not be captured depending on the scale and method of post-fire assessment (Smith and Hudak 2005; Holden *et al.* 2010; Kolden *et al.* 2012; Viedma *et al.* 2012). Such spatial heterogeneity is common, given mixed-severity fire regimes create a wide variation in fire effects that manifest as a fine-scale mosaic of stand-replacing and surface fire (Agee 1998; Arno *et al.* 2000). This variation is shaped by complex landscapes, including topography, moisture gradients, and the diversity and flammability of vegetation (Perry *et al.* 2011).

Vegetation response in the first post-fire year greatly depends on the extent of the damage to plants and soil above and below ground, which is a function of the severity of the fire and the resilience of the affected ecosystem (Neary *et al.* 1999;

Diaz-Delgado *et al.* 2003; Abella and Fornwalt 2015). The surge of new vegetation growth in the first year may seem incongruent with the initial burn severity classification (Lentile *et al.* 2007*a*) due to a boost in plant-available nitrogen (Stephan *et al.* 2012) and nutrients remaining in the ash layer (Neary *et al.* 1999); thus, it is important to monitor vegetation and soil recovery characteristics over time (Sankey *et al.* 2013; Berryman *et al.* 2014). The resilience of the ecosystem to the fire disturbance depends on specific conditions of the pre-fire environment such as vegetation type and density, and forest health such as drought or insect kill, taken into consideration with the scale and intensity of effects of the fire on the vegetation and soil (Idris *et al.* 2005; Schoennagel *et al.* 2008; Bowman *et al.* 2009; Perry *et al.* 2011).

Mappable ground cover components of interest in the post-fire environment are often green vegetation (GV), brown (senesced or dead) non-photosynthetic vegetation (NPV), charred material (char), ash and exposed mineral soil (Sá *et al.* 2003; Lewis *et al.* 2007; Smith *et al.* 2007*a*, 2007*b*; Eckmann *et al.* 2008). Of particular interest immediately post fire are char and ash, which are measurable biophysical variables that can be scaled between fires, as well as between field and remotely sensed images (Smith *et al.* 2005). The amount of char present and its persistence through the first post-fire year have been suggested as a suitable index of burn severity (Lentile *et al.* 2006; Quintano *et al.* 2013, 2017; Fernandez-Manso *et al.* 2016). Smith *et al.* (2007*a*, 2007*b*), Hudak *et al.* (2007) and Lentile *et al.* (2009) collectively used linear spectral mixture analysis to estimate the subpixel fraction of char to classify burn severity in African savannas and in multiple north-western United States forest ecosystems. Lentile *et al.* (2009) determined that char fraction outperformed dNBR (differenced Normalized Burn Ratio), when calculated from 1-year post-fire imagery, in predicting many of the field measures at both canopy and subcanopy scales. Hudak *et al.* (2007) observed in a study of eight north-western Rocky Mountain fires that changes in fractional vegetation and char cover either outperformed or were not significantly different from common severity spectral indices. Beyond linear spectral mixture analysis (SMA), several studies have employed multiple endmember spectral mixture analysis (MESMA) to monitor trajectories in post-fire recovery following field assessments of severity (Quintano *et al.* 2013, 2017; Fernandez-Manso *et al.* 2016).

Monitoring ecosystem patterns and post-fire response over years and decades has been conducted by employing temporal series of remotely sensed datasets (e.g. Hicke *et al.* 2003), predictive modelling (e.g. Kashian *et al.* 2006) and long-term field data collections (e.g. Romme *et al.* 2011), although the combination of these is uncommon. In the present study, we assembled a unique suite of post-fire field and remotely sensed data from three 2003 western Montana wildfires over 10 years. The combination of these datasets gave us a comprehensive view of changing soil and vegetation conditions in the burned area, pre-fire through 10 years post fire. Collectively, these data were used to assess whether any immediate field or remotely sensed indicators could forecast recovery over longer time periods and at a finer spatial resolution, building on related studies (e.g. Smith *et al.* 2007*a*; Lentile *et al.* 2009). In the present study, we focus on a definition of burn severity (Lentile *et al.* 2006; Parsons *et al.* 2010) that describes the longer-term effects of fires on vegetation and soils (Morgan *et al.* 2014). Specifically, we define burn severity as the effects of the fire on the ground surface, as measured by plant mortality and char cover. Although post-fire 'recovery' can have many implications and definitions (Bartels *et al.* 2016), for the purposes of this study, we concentrate on vegetation regrowth and change in ground cover, particularly the reduction in char, over the 10-year study period.

In this study, our objectives were to: (1) use data collected immediately post fire to confirm which factor(s) were most indicative of low, moderate and high burn severity; (2) evaluate the utility of high- and moderate-resolution remotely sensed imagery to discern post-fire char and other biophysical variables on the ground; (3) assess the contribution of the field measures to the degree and variability of burn severity and disturbance over a decade; and (4) analyse ecological change over 10 years using field data collected in 2013, and compare these data with the remotely sensed imagery to determine whether initial conditions are indicative of longer-term response.

Materials and methods

Study landscapes

The three study landscapes ranged from dry to wet mixed-conifer forest types in western Montana (Fig. 1) that were historically burned by mixed-severity fires at a fire return interval of ~80 years (Fischer and Bradley 1987). The driest landscape sampled was 2854 ha burned by the Black Mountain 2 Fire (henceforth referred to as Black Mountain) (centroid latitude and longitude: 46°50′29″N, 114°10′41″W; elevation: 1072–1743 m) on 8 August 2003. The Cooney Ridge Fire (centroid latitude and longitude: 46°40′10″N, 113°49′27″W; elevation: 1247–2167 m) also began on 8 August 2003 and burned 8589 ha of generally moist mixed-conifer forest. The third landscape containing the wettest mixed-conifer forest was burned by the Wedge Canyon Fire (centroid latitude and longitude: 48°54′22″N, 114°24′14″W; elevation: 1141–2414 m) that began on 18 July 2003 and burned 21519 ha.

Warm, dry sites at lower elevations throughout most of the Black Mountain Fire and much of the Cooney Ridge Fire were co-dominated by ponderosa pine (*Pinus ponderosa* Lawson and C. Lawson) and Douglas-fir (*Pseudotsuga menziesii* [Mirb.] Franco) in the *Pseudotsuga menziesii* habitat type series (Pfister *et al.* 1977; Cooper *et al.* 1991). The higher-elevation forests of the Wedge Canyon Fire on the western border of Glacier National Park were characterised by the *Abies lasiocarpa* habitat type series (Pfister *et al.* 1977; Cooper *et al.* 1991), with subalpine fir (*Abies lasiocarpa* [Hook.] Nutt.), Engelmann spruce (*Picea englemannii* Parry ex Englem.) and lodgepole pine (*Pinus contorta* Douglas ex Loudon). Lodgepole pine and western larch (*Larix occidentalis* Nutt.) also commonly occurred at many sites across all three fires. The soils across the Black Mountain and Cooney Ridge Fires were predominately gravelly silt loams and gravelly loams, whereas the Wedge Canyon Fire soils were sandy and silty glacial tills (USDA Natural Resources Conservation Service (NRCS) Web Soil Survey, http://websoilsurvey.nrcs.usda.gov/app; accessed 5 June 2017). Mean annual precipitation varied from 40 to

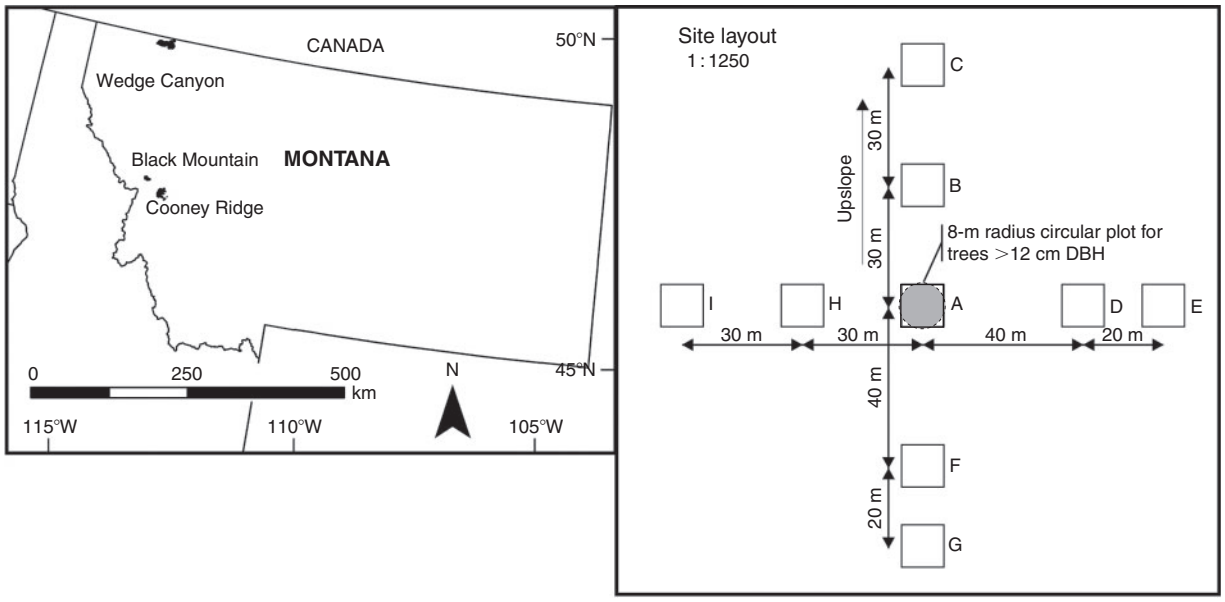

Fig. 1. The location of the 2003 wildfires in Montana with the site and plot layouts. Four sites were sampled on the Black Mountain Fire, seven at the Cooney Ridge Fire and five at the Wedge Canyon Fire. Each site had 9 plots and each plot had 15 subplots. (DBH, diameter at breast height.)

130 cm (Pfister *et al.* 1977) across the sites, mainly as a function of elevation. July is historically the warmest month at all sites with average annual high temperatures of 28–30°C and December is the coldest month with average annual low temperatures of −11 to −7°C (Montana Climate Office, years 1981–2010; http://climate.umt.edu; accessed 5 June 2017).

Field data

Field data were collected in 2003 and in 2004 to document burn severity and initial post-fire change. We assessed the functionality of mapping these components using airborne hyperspectral (HS) imagery collected immediately post fire. Decadal field data (collected in 2013) were used to evaluate changes in vegetative cover relative to pre-fire conditions. Anniversary Landsat data were acquired in 2002, 2003, 2004, 2007 and 2013 to map initial pre- and post-fire conditions and to approximate a trendline of vegetation response (the change in ground cover components (understorey GV, NPV, soil and char) over time) on the sites. High-resolution satellite QuickBird (QB) imagery from 2007 was used as an additional midpoint approximation of recovery between field data campaigns.

Post-fire soil and vegetation data were collected between 11 September and 22 October 2003 at four sites on Black Mountain, seven sites on Cooney Ridge and five sites at Wedge Canyon (Table 1). These sites were sampled as soon as safety and logistics allowed after the fires were officially out following established post-fire protocol (Lentile *et al.* 2007*b*), and were selected using the initial post-fire Burned Area Reflectance Classification (BARC) map (RSAC 2005) as a guide, and sample plots were then randomly located within areas burned across a range of low, moderate and high burn severities (Hudak *et al.* 2007) based on the predominant overstorey canopy condition: live, green (low); scorched, brown (moderate); or charred, black (high) (Table 2).

Each site was centred a random distance between 80 and 140 m from the nearest access road, within a consistent stand and burn severity condition. As described in more detail by Hudak *et al.* (2007), sampling at each site was spatially nested, consisting of nine 8 × 8-m plots (Fig. 1) with each plot comprising 15 1× 1-m subplots, for a total of 135 subplots per site. Plot centres were geolocated with a global positioning system (GPS) and differentially corrected. Sites were revisited from 12 to 15 July 2004 on the Black Mountain and Cooney Ridge Fires, and 13 to 14 August 2004 on the Wedge Canyon Fire. Field data were collected at only the site centre (A plot, 15 subplots per site). Five subplots per site were resampled 10 years after the fire (6 to 14 August 2013): one each at the centre of the A plots, and at the B, D, F and H plots resituated 30 m away in the same orthogonal directions as in 2003 (Fig. 1).

At the subplot scale, the percent cover of understorey GV, rock, mineral soil, ash, litter and any large organic matter (logs, branches or stumps) was ocularly estimated. The percentage char, if any, of each ground cover component was also recorded. The cover measures of ground materials were constrained to sum to unity, whereas the charred fractions of the ground materials were summed separately to get an aggregate estimate of percentage char. At the plot scale, litter and duff depths were measured, canopy closure was estimated using a convex spherical densiometer, canopy vegetation condition (% green, brown or black) was estimated at one plot per site, and a digital photo was taken for reference. To ensure consistency and repeatability between field crews, sampling protocol was calibrated daily and there was at least one common person on the field crew for each of the three field campaigns.

Field spectra

Multiple endmember spectra of ash, soil, rock, GV, NPV and charred NPV materials (Fig. 2) were collected in 2003 and 2004

Table 1. Remotely sensed image characteristics and acquisition dates for each platform, fire and image

Imagery	Platform (Landsat path/row)	Spectral bands used (nm)	Resolution (nominal)	Image dates
Probe-1 hyperspectral	Fixed-wing aircraft	432–2498[AB]	5.0 m after orthorectification	13, 14 Sept 03
Landsat 5 multispectral	Satellite	B1: 450–520	30 m	Black Mountain
		B2: 520–600		3 Aug 02
	Black Mountain: (41/27)	B3: 630–690		25 Oct 03
		B4: 760–900		25 Sept 04
	Cooney Ridge: (40/28)	B5:1550–1750		2 Sept 07
		B6: 2080–2350		Cooney Ridge
	Wedge Canyon: (41/26)			13 Sept 02
				2 Oct 03
				4 Oct 04
				11 Sept 07
				Wedge Canyon
				20 Sept 02
				25 Oct 03
				25 Sept 04
				16 Jul 07
Landsat 8 multispectral	Satellite	B2: 450–510	30 m	Black Mountain
		B3: 530–590		4 Oct 13
	(Same path/row as above)	B4: 640–670		Cooney Ridge
		B5: 850–880		11 Sept 13
		B6:1570–1650		Wedge Canyon
		B7: 2110–2290		20 Oct 13
QuickBird-2 multispectral	Satellite	B1: 450–520	2.6 m after orthorectification	Black Mountain
		B2: 520–600		11 Jul 07
		B3: 630–690		Cooney Ridge
		B4: 760–900		19 Jul 07
				Wedge Canyon
				29 Aug 07

[A]Excluding 1340–1480 and 1810–1970 nm at Black Mountain and Cooney Ridge Fires.
[B]Excluding 1280–1480 and 1735–1995 nm at Wedge Canyon Fire.

on cloud-free days within 2 h of solar noon within all burned areas using an ASD Pro-FR field spectroradiometer[1] (ASD 2002). Additional bright-target reference calibration spectra were acquired in a ~100-m^2 area of highly reflective light-coloured soil (such as a wide road intersection) on each fire. All field spectra were collected following the methods in Lewis *et al.* (2011), were compiled by fire and cover type, and are provided online for public use (http://www.frames.gov/partner-sites/assessing-burn-severity/spectral/; accessed 1 December 2016).

Airborne hyperspectral imagery

Airborne hyperspectral imagery was collected shortly after fires were contained in the fall (autumn) of 2003 (Table 1). The Probe-1 whisk-broom sensor was flown at 2100 m above ground level and data were collected along tracks 2.3 km wide and up to 28 km long from one end of the fire perimeter to the other, corresponding to a 512-pixel swathe width with an approximately 5 × 5-m ground instantaneous field of view at nadir. Image acquisition was between 1100 and 1300 hours local time to minimise shadowing; the solar zenith angle within 1 h of solar noon in the fall at this latitude was between 36 and 46° (45° and lower is desirable to reduce shadowing). Thirteen of the sixteen field sites fell within two flight lines each on the Black Mountain and Cooney Ridge fires and one flight line on the Wedge Canyon fire, whereas three sites fell outside the airborne imagery.

Satellite multispectral imagery

We used the Landsat Thematic Mapper (TM)-based burn severity dataset provided through the MTBS program (Eidenshink *et al.* 2007) to assign a burn severity class post-hoc to each site for comparison with our initial classes. MTBS data provide a standardised classification of unburned, low, moderate and high severities for all large fires based on pre- and 1-year post-fire dNBR data. We also acquired Landsat 5 images from years 2002–04 and 2007 and Landsat 8 images from 2013 that corresponded with post-fire anniversary dates (Table 1).

QuickBird-2 satellite imagery was acquired in the summer of 2007 (Table 1) over several large areas that encompassed all three fires in our study. The QB satellite collected data over a 16.8-km swath in five bands: a panchromatic band and four visible and near-infrared bands (DigitalGlobe, Longmont, Colorado, USA). QB imagery (2.4-m multispectral; 0.65-m panchromatic at nadir) allows fine-scale spatial discrimination of ground components in the post-fire environment. Images at each wildfire were delivered

[1]Trade names are provided for the benefit of the reader and do not imply endorsement by the USDA.

Table 2. Field site characteristics and the corresponding remotely sensed estimates for each field campaign: (a) 2003; (b) 2004; and (c) 2013

Data are sorted by mean char cover on the ground in 2003. MTBS refers to the Monitoring Trends in Burn Severity project; NPV is uncharred non-photosynthetic vegetation; GV is green vegetation; HS refers to the hyperspectral imagery; nd indicates no data

Fire, site	Extended MTBS burn severity	Char	Soil	NPV	GV	Ash	Black crown	Brown crown	Green crown	Landsat char	Landsat soil	Landsat NPV	Landsat GV	HS char	HS soil	HS NPV	HS GV
(a)			2003 Ground cover (%)				2003 Crown cover (%)						2003 Image estimates (%)				
Wedge Canyon 4	High	96	32	2	0	0	46	0	0	42	70	29	1	91	9	0	0
Black Mtn. 1	High	91	57	0	0	32	20	0	0	3	69	9	22	64	31	1	4
Cooney Ridge 1	High	91	66	0	1	13	9	8	0	87	16	84	0	56	36	8	0
Wedge Canyon 2	High	89	72	3	1	0	15	0	0	50	59	36	4	nd	nd	nd	nd
Wedge Canyon 1	Moderate	70	40	7	3	12	18	46	0	77	3	86	11	nd	nd	nd	nd
Cooney Ridge 5	Moderate	67	51	6	1	1	13	41	2	3	52	3	45	49	34	8	9
Cooney Ridge 4	Low	67	47	8	0	3	0	0	50	19	23	30	47	24	31	14	31
Cooney Ridge 3	Low	63	48	20	0	6	36	2	0	21	42	31	27	48	36	8	8
Cooney Ridge 6	Low	62	16	13	4	0	0	0	76	0	46	0	54	46	32	2	21
Cooney Ridge 7	Low	58	92	0	0	5	0	0	0	95	6	94	0	nd	nd	nd	nd
Cooney Ridge 2	Low	54	22	19	0	5	0	39	46	1	26	3	71	0	31	11	58
Wedge Canyon 3	Moderate	53	25	17	2	0	0	17	30	14	52	30	18	44	32	17	6
Black Mtn. 3	Low	53	30	3	0	1	0	33	2	12	27	50	23	43	55	0	2
Black Mtn. 2	Low	50	28	14	0	12	9	28	5	8	49	11	41	46	36	3	15
Wedge Canyon 5	Low	39	19	32	11	1	15	17	13	4	61	6	33	30	31	20	20
Black Mtn. 4	Low	28	73	16	1	1	0	2	17	42	38	47	15	47	38	9	6
(b)			2004 Ground cover (%)				2004 Crown cover (%)				2004 Image estimates (%)						
Wedge Canyon 4	High	69	19	4	15		21	0	0	46	18	56	26				
Black Mtn. 1	High	79	72	3	6		42	0	0	18	56	21	23				
Cooney Ridge 1	High	66	55	28	1		8	21	0	85	14	86	0				
Wedge Canyon 2	High	82	35	6	1		10	0	0	95	7	93	0				
Wedge Canyon 1	Moderate	42	11	44	12		6	23	0	71	4	85	10				
Cooney Ridge 5	Moderate	44	31	48	4		23	37	0	11	47	14	39				
Cooney Ridge 4	Low	42	32	28	24		0	0	62	15	18	20	62				
Cooney Ridge 3	Low	67	57	6	15		33	5	7	17	36	22	42				
Cooney Ridge 6	Low	13	7	73	12		5	16	50	0	52	0	48				
Cooney Ridge 7	Low	35	82	2	12		0	0	0	70	13	82	5				
Cooney Ridge 2	Low	21	4	57	21		4	24	35	0	32	0	68				
Wedge Canyon 3	Moderate	40	11	26	25		0	6	12	27	14	39	47				
Black Mtn. 3	Low	13	9	60	20		23	51	6	13	24	29	47				
Black Mtn. 2	Low	18	4	72	11		57	16	11	22	26	28	45				
Wedge Canyon 5	Low	6	3	18	74		5	5	10	3	17	8	75				
Black Mtn. 4	Low	26	29	4	65		0	5	11	24	21	35	45				
(c)			2013 Ground cover (%)				2013 Crown cover (%)				2013 Image estimates (%)						
Wedge Canyon 4	High	11	0	53	47		29	0	0	19	0	25	75				
Black Mtn. 1	High	6	8	34	58		46	0	0	63	38	0	0				
Cooney Ridge 1	High	0	15	29	56		6	0	0	51	6	70	24				
Wedge Canyon 2	High	7	14	19	67		32	0	0	51	5	62	33				

(*Continued*)

Table 2. (Continued)

Fire, site	Extended MTBS burn severity	Char	Soil	NPV	GV	Ash	Black crown	Brown crown	Green crown	Landsat char	Landsat soil	Landsat NPV	Landsat GV	HS char	HS soil	HS NPV	HS GV
Wedge Canyon 1	Moderate	nd	nd	nd	nd		nd	nd	nd	63	1	83	16				
Cooney Ridge 5	Moderate	4	1	24	75		25	1	1	33	0	41	60				
Cooney Ridge 4	Low	1	3	41	56		4	1	43	26	0	47	53				
Cooney Ridge 3	Low	12	4	28	68		6	1	3	45	0	54	47				
Cooney Ridge 6	Low	7	1	30	68		10	3	35	2	1	4	96				
Cooney Ridge 7	Low	0	61	6	29		0	0	0	68	6	82	12				
Cooney Ridge 2	Low	3	1	53	44		1	0	55	5	2	9	90				
Wedge Canyon 3	Moderate	5	2	16	82		0	0	39	3	7	32	61				
Black Mtn. 3	Low	3	7	58	35		5	0	3	49	8	73	19				
Black Mtn. 2	Low	5	0	31	69		27	0	30	2	15	5	81				
Wedge Canyon 5	Low	0	0	17	83		6	2	30	26	8	46	46				
Black Mtn. 4	Low	1	6	31	63		0	2	15	23	38	54	8				

as multiple geotiff files that were combined into radiometrically corrected and orthorectified image mosaics.

Processing methods

Image and field spectra processing steps are summarised in a flowchart in Fig. 3.

Airborne image preprocessing

Before delivery, the airborne hyperspectral data were converted to reflectance using *FLAASH* (Fast Line-of-sight Atmospheric Analysis of Spectral Hypercubes) (FLAASH Spectral Sciences, Inc., Burlington, Massachusetts, USA) (Black Mountain and Cooney Ridge Fires) or *ACORN 4.0* (Atmospheric Correction Now; AIG 2002) (Wedge Canyon Fire) by the image provider. Atmospheric conditions were more favourable at the Wedge Canyon Fire situated more than 200 km north of the other two fires, where smokier conditions demanded different atmospheric correction techniques. All reflectance data were further refined with a Radiative Transfer Ground Calibration (RTGC) (Clark *et al.* 2002). To ensure that all images were comparable, reflectance data were also corrected using an Empirical Line Calibration (ELC), which minimises atmospheric and illumination effects by standardising them across all bands in the image (Richards and Jia 1999). Wavebands between 1340–1480 and 1810–1970 nm were eliminated from all images because of atmospheric water absorption in these bands, and band 2512 nm was removed for noise, leaving 119 bands for analysis. The excluded water absorption ranges were slightly wider for the Wedge Canyon imagery: 1280–1480 and 1735–1995 nm, leaving 108 bands for analysis.

On-board GPS and inertial measurement unit geolocation data, together with a 30-m digital elevation model, were used for georeferencing the imagery. On examination, the georeferenced images were distorted; therefore, we warped the imagery with a high density of ground control points (60–130 per flightline, proportional to area) via Delauney triangulation. Orthorectified digital orthoquads (1-m) were used as base imagery, necessitating resampling to 5-m resolution. No error statistics are reported for Delauney triangulation; however, accuracy was thoroughly checked between the warped images and the base images to visually confirm that features (such as road intersections) easily recognised on the ground and independently geolocated with a resource-grade GPS (i.e. with differential correction) spatially corresponded.

Multiple endmember spectral mixture analysis

In linear SMA, the solution of a linear model enables the calculation of the relative proportions that a given cover type contributes to pixel reflectance (Roberts *et al.* 1993; Settle and Drake 1993). The linear mixture model (eqn 6 in Cochrane and Souza 1998) is defined by:

$$R_i = \sum_{j=1}^{n} \left(R_{i,j} f_j\right) + e_i \qquad (1)$$

where R_i is the spectral reflectance of the ith spectral band of a pixel; $R_{i,j}$ is the spectral reflectance of endmember j in band i; f_j

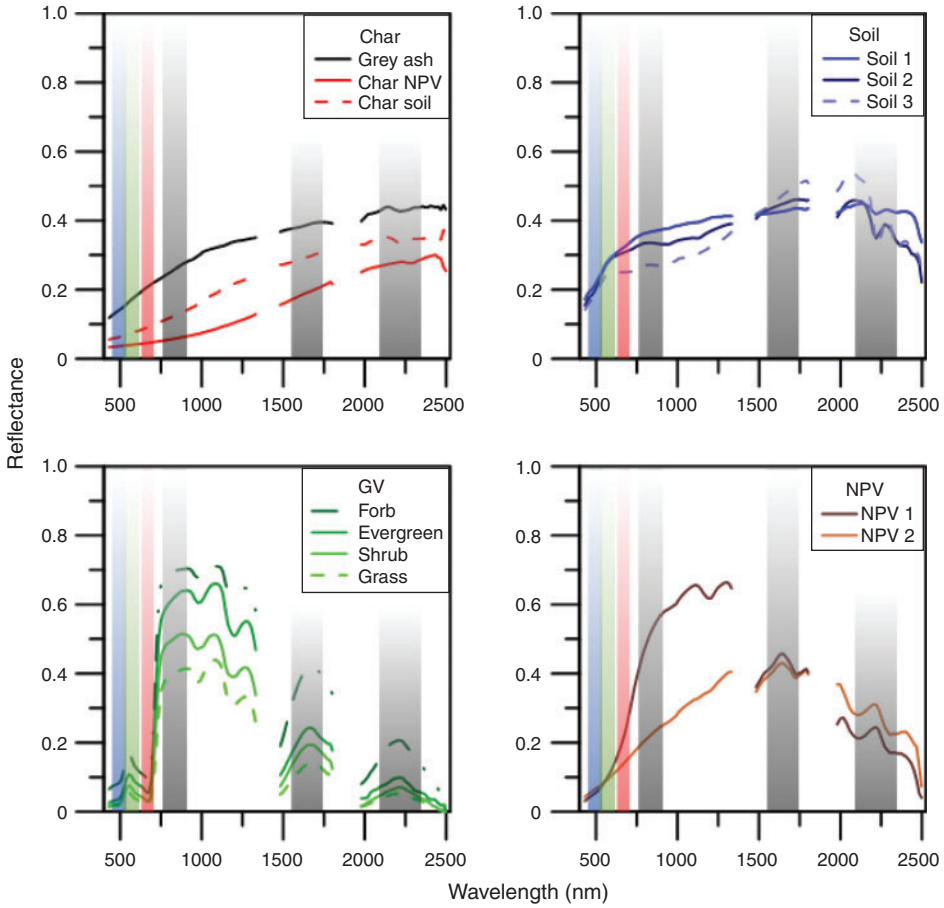

Fig. 2. The four spectral libraries that were used for the multiple endmember spectral mixture analysis (MESMA). Atmospheric water absorption bands were removed at ~1400 and 1900 nm. GV is green vegetation; NPV is non-photosynthetic vegetation. The three soil samples were from different road intersections, all bright, uncharred soils. Blue, green, red and near-infrared (grey) Landsat and QuickBird bands are shaded, as well as two short-wave-infrared Landsat bands (grey).

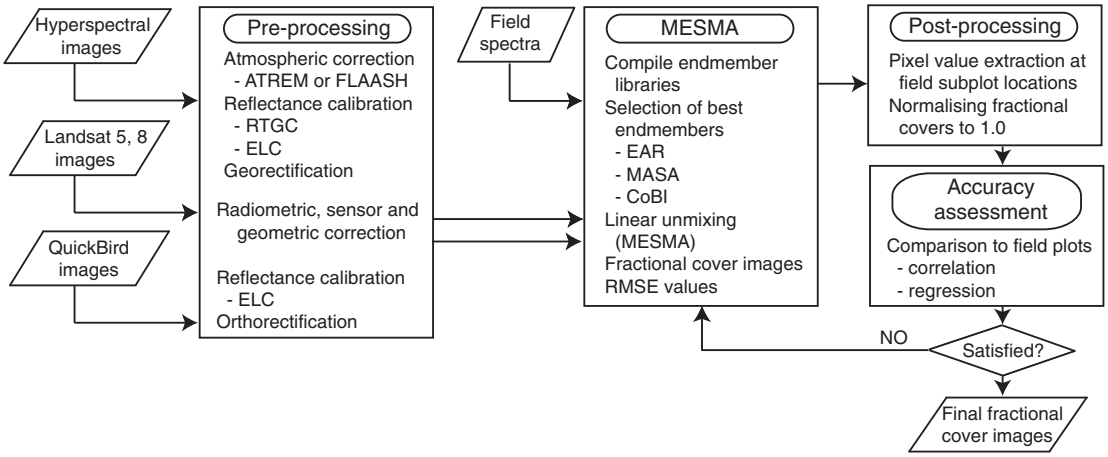

Fig. 3. An overview of the endmember selection and image processing steps. (ATREM, Atmospheric Removal Program; *FLAASH*, Fast Line-of-sight Atmospheric Analysis of Hypercubes; RTGC, radiative transfer ground calibration; ELC, empirical line calibration; MESMA, multiple endmember spectral mixture analysis; RMSE, root mean square error; EAR, endmember average RMSE; MASA, minimum average spectral angle; CoBI, count-based endmember selection index.)

Table 3. Comparing the change in mean ground and canopy cover percentages at the spatially coincident A plots for all fires; standard error in parenthesis

The burn severity classes are based on the Monitoring Trends in Burn Severity (MTBS) extended assessment. In 2013, all plots but one were resampled (one moderate-severity plot was inaccessible). Cover fractions besides char sum to 100%. NPV is uncharred non-photosynthetic vegetation; GV is green vegetation. The sum of the canopy vegetation components in a row is the mean canopy cover of that burn severity class

Year, burn severity	Char (%)	Ash (%)	Soil (%)	NPV (%)	GV (%)	Canopy char (%)	Canopy NPV (%)	Canopy GV (%)
2003								
High ($n=4$)	92 (1.5)	12 (7.6)	57 (8.7)	1 (0.7)	<1 (0.2)	23 (8.1)	2 (2.0)	0 (0)
Moderate ($n=3$)	64 (5.2)	5 (3.9)	39 (7.5)	10 (3.4)	2 (0.8)	10 (5.3)	35 (9.1)	11 (9.6)
Low ($n=9$)	53 (4.2)	4 (1.3)	42 (8.7)	14 (3.2)	2 (1.3)	7 (4.1)	13 (5.3)	23 (9.1)
2004								
High ($n=4$)	74 (3.9)	4 (2.1)	46 (11.5)	10 (5.9)	6 (3.3)	20 (7.7)	5 (5.1)	0 (0)
Moderate ($n=3$)	42 (1.2)	1 (0.1)	18 (6.7)	39 (6.7)	14 (6.1)	10 (6.8)	22 (8.8)	4 (4.1)
Low ($n=9$)	27 (6.3)	2 (1.3)	25 (9.3)	36 (9.9)	28 (8.0)	14 (6.6)	14 (5.4)	21 (7.4)
2013								
High ($n=4$)	6 (2.3)	0 (0.0)	10 (3.4)	34 (7.1)	57 (4.2)	28 (8.3)	0 (0)	0 (0)
Moderate ($n=2$)	5 (0.7)	0 (0.0)	2 (0.3)	20 (4.0)	79 (3.7)	13 (12.6)	<1 (0.3)	20 (18.9)
Low ($n=9$)	4 (1.3)	0 (0.0)	9 (6.5)	33 (5.4)	57 (5.9)	7 (2.8)	1 (0.4)	24 (6.6)

is the fraction of endmember j; and e_i is the error in band i. MESMA utilises the same linear model as SMA, but the endmembers mapped vary on a pixel-by-pixel basis rather than the strict SMA constraint of each pixel containing the same endmembers (Roberts *et al.* 1998). MESMA code is part of *VIPER* (Visualisation and Image Processing for Environmental Research) *Tools* (VIPER Tools, Santa Barbara, CA, USA).

VIPER Tools have a built-in, iterative endmember process that allows the selection of the most representative endmembers relative to the objects of interest (Tompkins *et al.* 1997; Dennison and Roberts 2003). Related yet spectrally distinct endmembers (e.g. GV functional types) may be combined into a single endmember class. MESMA also allows for variations present within the same material, such as different soil types, which can all be accounted for within a single 'soil' spectral library. Computational intensity is increased with a high number of endmembers, whereas too few may result in large residuals (Dennison *et al.* 2004; Li *et al.* 2005; Roth *et al.* 2012).

It has been suggested that natural and disturbed systems are best modelled by two- or three-endmember models (Powell and Roberts 2008; Wang *et al.* 2012); thus, we used *VIPER Tools* to investigate two-, three- and four-endmember models to estimate char, soil, GV and NPV cover and photometric shade after wildfire. A large set of potential endmembers (59 unique endmembers, with 5–30 replicates of each) was iteratively narrowed down. Endmembers were first sorted into broad classes: GV, NPV, soil and char. Within the GV class, multiple species of deciduous and conifer trees, shrubs, forbs and grasses were considered to account for spectral variability, particularly in the sparsely vegetated post-fire environment (Okin *et al.* 2001). The NPV class consisted of various uncharred litter and bark materials. Uncharred soil and rock made up the soil class, and a separate char class had dark char, and charred soil and NPV. Two to four 'best' endmember signatures were selected for each category based on how well they spectrally represented the cover class; the same set of endmembers was used on all three fires (Fig. 2).

MESMA was applied to the 20 post-fire HS image strips. The minimum allowable endmember fraction, maximum allowable endmember fraction, and maximum allowable shade fraction were set to the default values of −0.05, 1.05 and 1.0 respectively, and the maximum root-mean-square error (RMSE) was 0.05. Typically, the shade fraction is set at 0.8, but because of low albedo in some areas of the HS imagery due to tall trees and topographic shading (Dennison *et al.* 2004; Yang *et al.* 2015), and the preponderance of dark char, we were able to extract more spectral information by increasing the shadow allowance. By analysing the models that mapped the greatest percentage of the area of interest, we were able to iteratively select the best endmembers and endmember combinations (Youngentob *et al.* 2011) until the best model results (i.e. accurate fractional estimates over the greatest area) were obtained.

The same endmember bundles were used for MESMA modelling of the Landsat and QB images. QB only has four spectral bands; thus, we were constrained to two- or three-endmember models. Modelling efforts were most successful via a series of two-endmember models in which each endmember component was estimated separately (plus shade); the relative cover fractions of each pixel were calculated by combining the separate model results.

Accuracy assessment

Pixel values from the fractional cover images were extracted at the field subplot locations (i.e. 135 subplots per site). These data were aggregated along with the field data at the plot (15 subplots per plot), and site (nine plots per site) scales. Most sample distributions were non-normal (via the UNIVARIATE procedure in *SAS* (SAS Institute Inc. 2003)); therefore, non-parametric statistical tests were used for subsequent analyses. The MESMA cover estimates of char, soil, GV and NPV from the remotely sensed imagery were compared with the 2003, 2004 and 2013 field data to evaluate the ability to make accurate estimations (2003 data) and predictions (2004 and 2013 data). Direct (e.g. 2003 image and field data) and predictive (e.g. 2003 image and 2013 field data) correlations among the variables were assessed using the non-parametric Spearman rank correlation test (SAS Institute Inc. 2003); Spearman correlation coefficients (ρ) are reported. A significance level of 0.05 was used for all statistical tests.

Table 4. Direct (e.g. 2003 image and 2003 field data) and predictive (e.g. 2003 image and 2013 field data) Spearman rank correlation coefficients for: (a) 2003; (b) 2004; and (c) 2013 field cover measures

HS refers to hyperspectral imagery; NPV is uncharred non-photosynthetic vegetation; GV is green vegetation. Bold values are significant at $P < 0.05$; correlation coefficients with an absolute value of <0.1 are denoted by '<0.1'

Image fractional cover estimates	Char (%)	Soil (%)	NPV (%)	GV (%)	Canopy GV (%)
(a)			2003 Field cover measures		
HS (2003, $n = 13$ sites)					
Char	**0.60**	**0.62**	**−0.59**	<0.1	**−0.76**
Soil	−0.37	0.41	<0.1	−0.21	<0.1
NPV	−0.38	−0.17	**0.68**	0.44	0.54
GV	−0.35	**−0.55**	**0.61**	0.11	**0.75**
Landsat 5 (2003, $n = 16$ sites)					
Char	0.25	**0.67**	−0.39	<0.1	**−0.55**
Soil	0.10	−0.22	<0.1	0.10	−0.13
NPV	<0.1	0.61	−0.39	<0.1	**−0.53**
GV	−0.38	**−0.63**	**0.60**	−0.11	**0.70**
(b)			2004 Field cover measures		
HS (2003, $n = 13$ sites)					
Char	**0.74**	**0.61**	−0.49	**−0.66**	**−0.78**
Soil	−0.15	0.21	0.13	−0.12	0.13
NPV	−0.23	−0.20	−0.11	**0.62**	0.50
GV	−0.47	−0.44	0.49	0.31	**0.75**
Landsat 5 (2004, $n = 16$ sites)					
Char	0.56	**0.51**	**−0.51**	−0.37	**−0.59**
Soil	<0.1	<0.1	0.28	−0.10	0.25
NPV	0.45	0.44	−0.43	−0.32	**−0.60**
GV	**−0.71**	**−0.72**	0.49	**0.72**	**0.84**
(c)			2013 Field cover measures		
HS (2003, $n = 13$ sites)					
Char	0.39	0.24	−0.12	−0.03	**−0.88**
Soil	<0.1	0.48	−0.12	0.03	0.23
NPV	−0.47	−0.22	−0.53	0.51	**0.65**
GV	−0.13	−0.46	−0.09	0.31	**0.84**
Landsat 5 (2003, $n = 16$ sites)					
Char	−0.23	**0.58**	−0.31	−0.36	**−0.52**
Soil	**0.62**	−0.43	<0.1	**0.54**	0.18
NPV	−0.31	**0.74**	−0.19	−0.46	−0.48
GV	0.12	**−0.60**	0.32	0.33	**0.76**
Landsat 8 (2013, $n = 16$ sites)					
Char	−0.38	**0.56**	−0.35	−0.34	**−0.81**
Soil	−0.30	0.14	<0.1	<0.1	<0.1
NPV	−0.45	**0.64**	−0.29	−0.36	**−0.82**
GV	0.41	**−0.80**	0.20	0.36	**0.76**

Results

Initial burn severity condition

At the plot scale (~10 m), we characterised the variability of fire effects on soil and understorey vegetation and canopy condition. In 2003, plots classified as MTBS high burn severity had 92% average char cover and a trace of understorey GV, whereas moderate and low burn severity plots had less char (64 and 53% respectively) and sparse understorey GV cover (2%) (Table 3). Understorey GV was not a differentiating indicator of fire effects immediately after the fire. However, based on the 2004 extended assessment of coincidental plots, understorey GV increased considerably to 14% on moderate burn severity plots and 28% on low burn severity plots. Char was still most prominent on high burn severity plots (74%) in 2004 and less prevalent on the moderate (42%) and low (27%) burn severity plots (Table 3). Remaining canopy cover was low on all sites (25–56%), with high-severity sites dominated by charred canopy (23%), moderate-severity sites dominated by NPV (including dead and scorched) canopy (35%), and low-severity sites dominated by green canopy (23%).

Correlation between field and remotely sensed variables

At the site scale ($n = 13$ sites where HS imagery was available), there were significant positive correlations between three field components (2003) and their remotely sensed counterparts (Table 4a): char cover and the HS char estimate ($\rho = 0.60$); NPV cover and the HS NPV estimate ($\rho = 0.68$); and green canopy cover and the HS GV estimate ($\rho = 0.75$). The most significant correlation between Landsat and field data was canopy GV ($\rho = 0.70$). We also found correlations were split by inorganic and

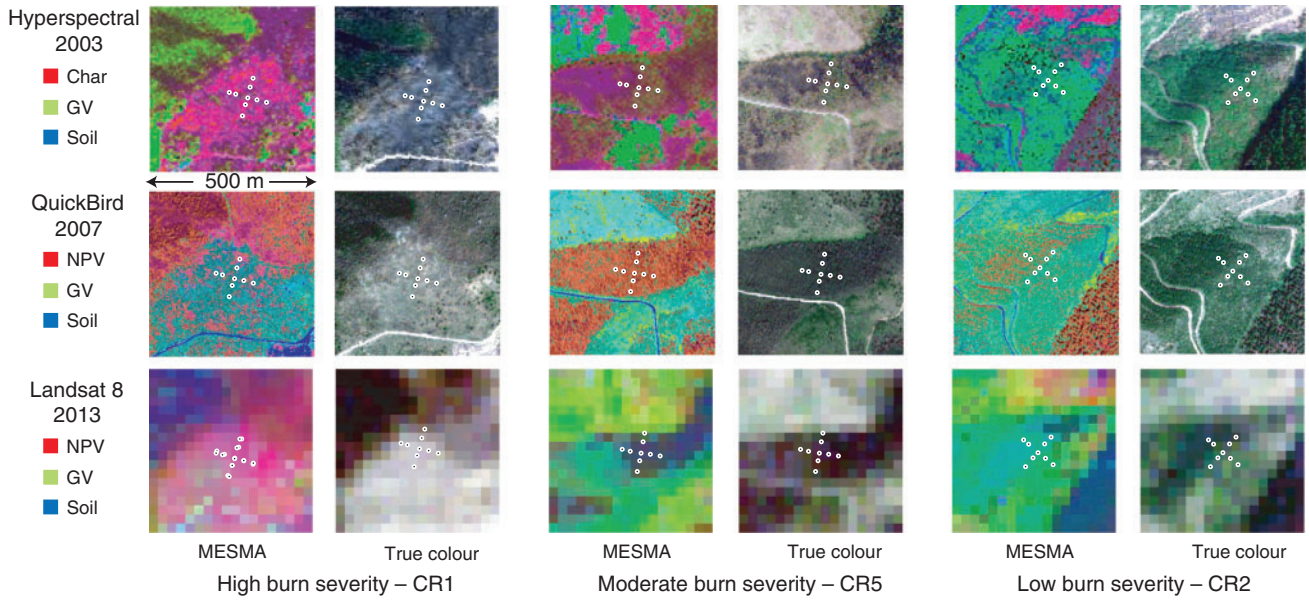

Fig. 4. A comparison of the immediate post-fire images (2003) and those collected 4 years later (2007) and 10 years later (2013) across a range of burn severities. The multiple endmember spectral mixture analysis (MESMA) results are shown next to the true colour (red, green, blue) images. Resolution (pixel size) varied by image type: hyperspectral (5 m); QuickBird (2.6 m); Landsat (30 m). All three site subsets are from the Cooney Ridge (CR) Fire, sites 1, 5, and 2 with plot locations overlaid; site characteristics are shown in Table 2. (GV, green vegetation; NPV, non-photosynthetic vegetation.)

organic cover classes (e.g. HS and Landsat char were correlated with soil cover, and HS and Landsat GV were correlated with NPV cover), as the cover variables logically aligned by broader cover classes such as inorganic or organic, and charred or uncharred.

In 2004, the most notable direct correlations were between Landsat GV with GV on the ground (understorey) and in the canopy ($\rho = 0.72$ and 0.84 respectively) (Table 4b). For the first post-fire year, HS char remained positively correlated with char ($\rho = 0.74$) and soil ($\rho = 0.61$) on the ground, and negatively correlated with GV on the ground or in the canopy ($\rho = -0.66$ and -0.78 respectively) (Table 4b). Hyperspectral GV was correlated with canopy GV ($\rho = 0.75$). The char and soil correlations remained mostly consistent from 2003 to 2004, whereas the Landsat GV correlations were stronger with vegetation regrowth.

Trends in site recovery across burn severity classifications

The change in site characteristics over the first 4 years (2003–07) on three representative sites after the Cooney Ridge wildfire (Fig. 4) implied a significant shift in dominant cover from char to NPV and GV, regardless of the MTBS burn severity classification. Initially, char was prevalent on the high burn severity site, with more mixed components on the moderate burn severity site, and a prevalence of understorey GV on the low burn severity site. The transformation in site characteristics was apparent in the images: char was mostly replaced by soil and NPV, and on the high and moderate burn severity sites, GV (likely canopy GV from trees that later died) was replaced primarily by NPV. On the low burn severity site, GV was mixed with NPV rather than char after 4 years.

In 2007, when the QB and Landsat midpoint images were acquired, the trends from our field data (solid lines on Fig. 5) show an estimate of 40% understorey GV cover on moderate and low burn severity sites and closer to 20% on high burn severity sites. Understorey GV was seemingly underestimated in the QB imagery across all burn severities, whereas the Landsat data overestimated understorey GV on the low-severity sites (Fig. 6). Soil, char and NPV ground cover were closely approximated on the low- and moderate-severity sites by both QB and Landsat in 2007; on the high-severity sites, however, soil and char were underpredicted by the remotely sensed images and NPV was overpredicted (Fig. 6).

Ten years after the fires in 2013, there was 10% or less char or exposed soil left on the plots, and the primary cover classes were NPV (20–34%) and understorey GV (~60–80%) (Table 3; Fig. 4). These data indicate a significant trend towards site recovery regardless of initial burn condition. Interestingly, the canopy data do not reflect as considerable change as do the ground data; canopy char on the high-severity sites (20–30%) and canopy GV on the low-severity sites (20–25%) are similar across 10 years, whereas the most notable change is the loss of canopy NPV as nearly all the scorched, brown needles fell from trees (Table 3).

The 2013 Landsat data underpredicted understorey GV and overpredicted char across all burn severity classes (Fig. 6). Although there was little char left on the ground, there was still nearly 30% charred (black) canopy remaining on the high-severity sites in 2013 (Table 3). Correspondingly, there was significant GV on the ground, but less than 25% in the canopy. Moderate-spatial-resolution sensors like Landsat will often detect occluding canopy rather than occluded surface condition (Hudak *et al.* 2007), which would account for the prediction discrepancies. Landsat estimates of NPV and especially soil cover were more accurate (Fig. 6).

The only significant direct correlation between 2013 Landsat 8 data and the ground data was between Landsat GV and canopy GV ($\rho = 0.76$); Landsat 8 char and NPV were negatively

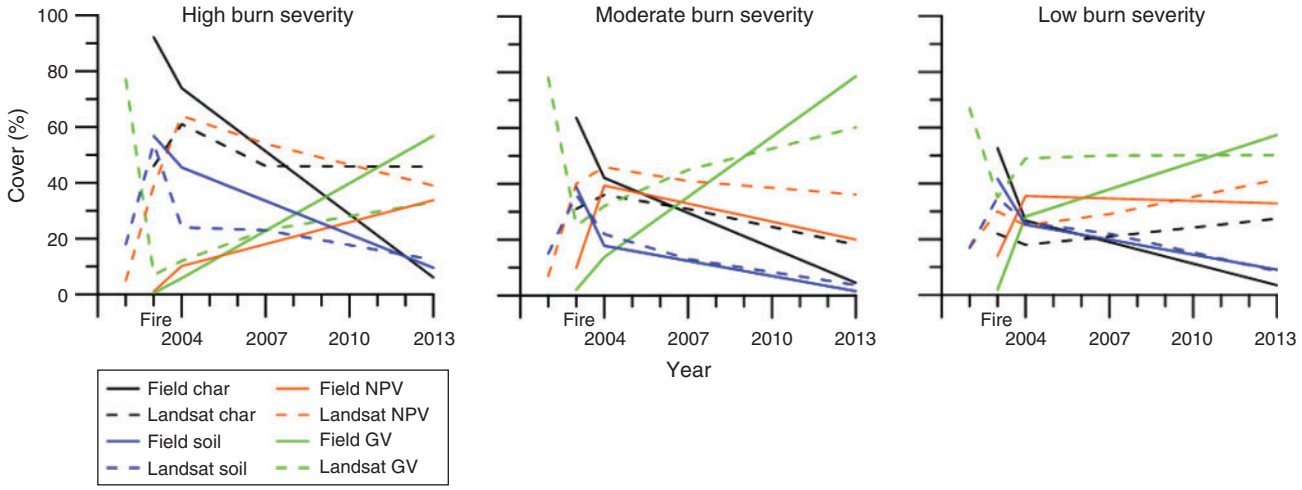

Fig. 5. Means of the understorey ground cover field measures (solid lines) in 2003, 2004 and 2013 by Monitoring Trends in Burn Severity (MTBS) burn severity classes: (*a*) high; (*b*) moderate; and (*c*) low burn severity. The mean Landsat estimates from the multiple endmember spectral mixture analysis (MESMA) are shown as dashed lines. (GV, green vegetation; NPV, non-photosynthetic vegetation.)

correlated with canopy GV ($\rho \sim -0.8$). The 2003 Landsat data indicated a few predictive correlations: between char and soil measured on the ground and in the image ($\rho \sim 0.6$) and between Landsat GV and canopy GV ($\rho = 0.76$). Predictive correlations between the 2003 HS remotely sensed estimates and the 2013 field data were very similar to the 2013 Landsat 8 data, and were significant between canopy GV and HS char ($\rho = -0.88$), HS NPV ($\rho = 0.65$) and HS GV ($\rho = 0.84$) (Table 4c).

Discussion

The post-fire environment in the first year

We were able to reasonably estimate char cover on all sites from the HS imagery because of its cover dominance and spectral separability (Figs. 4, 6). The significant correlations ($\rho = 0.6$–0.74) between image-predicted char and the field measures in the first post-fire year (Table 4a, b) combined with the prevalence and persistence of char lead us to confirm that char is a consistent indicator of burn severity, which is in agreement with prior studies in other ecosystems (French *et al.* 2004; Smith *et al.* 2005; Veraverbeke *et al.* 2012; Quintano *et al.* 2013). The data distributions in the first full year of the present study were bimodal, as the low and moderate sites had comparable cover fractions of char, understorey GV and NPV and soil, whereas the exclusively charred high burn severity sites were more distinctly separable (Table 3, Fig. 4). Quintano *et al.* (2017) also found post-fire data collected after a Mediterranean wildfire to more naturally separate between two classes: low–moderate and high, rather than the three classes commonly used (low, moderate and high).

There was more char remaining on the high burn severity plots 1 year after the fire (74%) than on the moderate burn severity plots immediately after the fire (64%). The amount of residual char through the first post-fire year and beyond is a measurable biophysical variable that can be scaled between fires (Smith *et al.* 2010), between field and remotely sensed images (Quintano *et al.* 2017), and may be used to forecast ecological response and future vulnerability, an area of remote sensing that will likely see further investigation (Smith *et al.* 2014). Lentile *et al.* (2009) suggested fractional char cover as estimated via spectral mixture analysis of Landsat Enhanced Thematic Mapper Plus (ETM+) data was the best correlate to 1-year post-fire field measures, thus providing a physical indicator of eventual site recovery. This result was also confirmed in later studies (Hudak *et al.* 2013).

Contribution of other factors to burn severity and disturbance

Negligible understorey GV was found immediately after the fire; however, more overstorey GV (tree canopy) remained: 23 and 11% on the low and moderate burn severity plots (Table 3). Moderate severity sites had 35% NPV canopy cover in 2003, which decreased to 22% by 2004, and almost completely disappeared by 2013. Scorched needles in the canopy and subsequently on the ground are a signature of moderate burn severity.

Because our study objectives concentrated on understorey vegetation and ground cover, we only have tree crown condition data (e.g. green, scorched, or charred) on one plot per site per field year. Although most of the canopy is consumed or blackened in high burn severity areas, tree crowns remaining on the low and moderate burn severity sites can occlude fire effects on soils, which may be disproportionately decoupled from the overstorey condition immediately post fire (e.g. prolonged soil heating due to a sustained, low-intensity surface fire that consumes much of the duff layer (Ryan 2002)). We observed these conditions at two Cooney Ridge field sites (4 and 6) that had 100% green crown yet 67 and 62% ground char cover (Table 2). Canopy occlusion of fine-scale ground effects likely further confounded our remotely sensed estimates on other sites as well.

Neither NPV nor soil cover were diagnostic indicators of burn severity immediately after the fire. Uncharred NPV cover was low (<15%) on all sites in 2003 and soil cover was somewhat ubiquitous (40–60%), regardless of burn severity (Tables 2 and 3). Quintano *et al.* (2013) also confirmed that

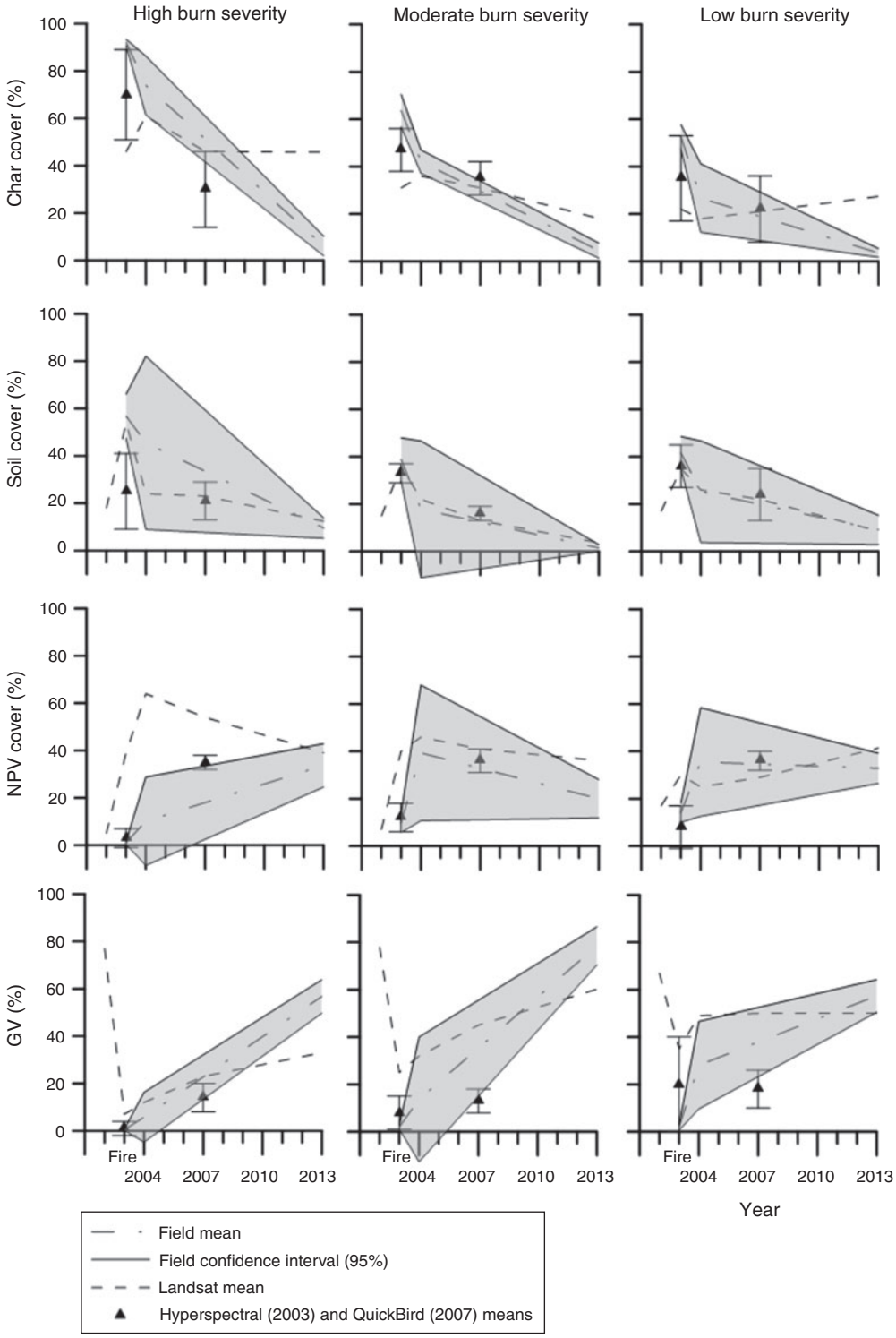

Fig. 6. Field site characteristics visually compared with 2002–04 and 2007 Landsat 5, 2013 Landsat 8, 2003 hyperspectral and 2007 QuickBird fractional cover image estimates. A 95% confidence interval is shaded around the field means (understorey ground cover) to illustrate how well the image estimates compare with the range of variability measured in the field. (GV, green vegetation; NPV, non-photosynthetic vegetation.)

the amount of soil cover did not change predictably among burn severity classes. Soil cover decreased by 20–50% in 2004, yet was still a primary cover factor (Table 3); however, 10 years after the fire, less than 10% exposed soil remained on any of the plots. The change in exposed soil due to a disturbance (or recovery from a disturbance) can be an indication of the degree of disturbance (Page-Dumroese *et al.* 2009), such as after a wildfire or logging.

Vegetation recovery was rapid regardless of burn severity classification

The Landsat MTBS extended assessment classes suggested there were far more low burn severity sites than we initially assessed. Even though these sites were mostly charred in 2003 (>50%), significant vegetation recovery occurred in the first post-fire year, a trend that was sustained for 10 years (Figs. 5, 6). This is consistent with Bataineh *et al.* (2006), who found that even in lightly burned areas, removal of forest canopy or litter stimulated understorey vegetation growth for more than a decade following a wildfire in Arizona.

While soil and char cover decreased consistently over time, NPV and understorey GV increased; the rates of increase varied depending on the initial burn severity condition (Figs. 5, 6). Most notable was the increase in understorey GV on the high burn severity sites from 0 to 60% over the 10-year study period. This is comparable with findings of Shive *et al.* (2013), who found four-time greater understorey cover in areas burned at high severity compared with low severity 8 years after the Rodeo–Chediski wildfire in Arizona, and Wittenberg *et al.* (2007), who measured vegetation cover equivalent to pre-fire levels 5 years after a Mediterranean wildfire. Idris *et al.* (2005) reported following wildfires in Borneo and in China, the recovery time for areas burned at high severity was also highly dependent on the scale of the fire – larger patches took longer to recover. The relatively rapid understorey recovery we measured on these western Montana fires can partly be attributed to historical mixed-severity fire regimes in this region (Arno *et al.* 2000), which result in a mosaic of forest structure and plant communities, and often patchy fire effects.

As stated, we found inorganic variables changed more consistently and predictably during the post-fire period considered, while organic cover measures understorey GV and NPV responded non-linearly and exhibited greater discrepancies between the ground and canopy. Viedma *et al.* (1997) modelled asymptotic vegetation recovery over a decade in the Mediterranean using Landsat 5 data. The three field data points over a decade from our study are not sufficient to create a good fit, but it is possible to visualise that the green vegetation is increasing asymptotically (Figs. 5, 6).

Understorey GV and NPV cover replaced char and inorganic cover as primary ground cover 1 year after the fire on low burn severity sites (Fig. 5). We estimate this same benchmark of recovery occurred on the moderate burn severity sites approximately 2 to 3 years later, and another 3 to 4 years later (7 or more years after the fire) on the high burn severity sites (Fig. 5). As stated previously, the true shape of these recovery trajectories is almost certainly non-linear, as expected from a biological process (Peters *et al.* 2004), but importantly, the up-or-down tendencies in these basic post-fire projections are corroborated by the QB and Landsat estimates, substantiating the revegetation trends. At the scale of our study sites, recovery among the burn severity classes converged after 10 years in terms of major cover classes (Table 3, Fig. 5).

The shift and convergence of primary cover types over time emphasise the dynamic nature of the post-fire environment. Char is most prevalent immediately after the fire, but in the following decade, char is concealed by an abundance of NPV and understorey GV. Although none of the initial measures were statistically indicative of eventual understorey GV, HS char, HS NPV and HS GV estimates from 2003 were significantly correlated with the amount of canopy GV found in 2013. As expected, the absence of char and any presence of understorey GV immediately after the fire indicated a greater amount of understorey GV 10 years later (Table 4c). It is notable that initial remotely sensed HS estimates were sustained over a decade, suggesting their potential use for longer-term vegetation recovery predictions. The considerable presence of understorey GV and NPV 10 years post fire emphasises a productive vegetation response in the burned environments (Table 3).

Limitations of remotely sensed data for inferring burn severity

High-spatial- and spectral-resolution HS imagery allowed effective discrimination of fine-scale post-fire ground cover, especially char, as others have found (van Wagtendonk *et al.* 2004; Kokaly *et al.* 2007; Robichaud *et al.* 2007). The time lag between site burning, field sampling and image acquisition as well as the difference in conditions between sites (e.g. smoke) likely affected correlations between the image and field data across all sites, as described in detail by Hudak *et al.* (2007). Ideally, all data would be collected as temporally coincidentally as possible; however, field campaigns and tasked image collections are often challenging to coordinate, and we felt fortunate to have collected all initial data within 3 months of burning.

As supplied from the vendor, the HS image data were distorted even after georeferencing. To compare the field data with the image data at coincidental locations, warping and resampling the images was necessary. Although these intensive adjustments may have affected data at the subplot (1–5-m) scale, all field and image data were aggregated to the site scale (0.01 km^2) and we feel confident that the spatial variability and true means of the data were captured at this resolution on aggregation to the site level. The potential for misaligned data was further overcome by the unusually intensive ground sampling effort undertaken in the initial assessment, with 15 times as many 1-m^2 subplots per plot in 2003 compared with 2004 and 2013, over an area equivalent to nine Landsat pixels in 2003 and five pixels in 2004 and 2013. The initial sites were also situated randomly but well within large (0.1-km^2) patches of a given burn severity condition to minimise edge effects confounding the relationships to Landsat resolution imagery (Hudak *et al.* 2007).

We had some difficulty with shadowing and low albedo in the both the HS and QB images. Shadows are common in forested areas, and these study areas had significant topographic relief. Shadows were apparent from both tall trees and steep terrain, and the HS imagery was acquired from a fixed-wing aircraft, which added to off-nadir viewing angles, especially

compared with satellite imagery. Additionally, the burned sites averaged 65% char cover in 2003, which decreased the overall albedo of the images and thus spectral contrast (Rogan and Yool 2001). We compensated for some of the darkness and shadowing by allowing more shadow to be mapped as well as increasing the maximum allowable RMSE to 0.05 or 0.1 as needed. Overall mean RMSE for the MESMA modelling was low: 0.01–0.02. The Cooney Ridge QB image had the highest RMSE at 0.06. Adjusting the constraints of the MESMA model within *VIPER Tools* allowed more pixels to be mapped in several images.

QB data were acquired from the DigitalGlobe image archive (https://browse.digitalglobe.com/imagefinder; accessed 16 September 2016). QB is more often used as a 'ground truth' dataset in ecological studies (Willis 2015) and somewhat less often for high-level analysis (such as spectral unmixing) because of its broadband spectral resolution. It is worth noting that there is no conceptual reason why SMA cannot be applied to any type of calibrated, multispectral imagery. Arguably, the estimation of char, understorey GV and other ground-cover components is a more scalable method in the context of burn severity assessments than the much more commonly considered Normalized Burn Ratio (NBR) (Veraverbeke and Hook 2013). Indeed, the absence of a short-wave infrared (SWIR) band in QB and most other high-resolution imagery precludes the calculation of NBR. However, our primary intention in this study was to use the midpoint images (QB and Landsat) to validate the field data trends (Fig. 6), and both image types served that purpose well.

Conclusions

The rate of post-fire environmental change (e.g. increase in understorey GV and decrease in exposed char and soil) is high in the first year and slows with time. The initial post-fire conditions were highly spatially heterogeneous at the scale of our study, with the exception of sites burned at high severity, which were primarily charred. We found char cover to have considerable persistence; it remained the primary cover factor for high burn severity 1 full year after the fire. Although ~25–75% char remained on site in the first post-fire year across all burn severities, the ratio of understorey GV and NPV to char and soil cover was much higher after a growing season, indicating resurgence of the vegetative strata and consequent protection of the soil strata. An increase in NPV cover reduces the risk of soil erosion and runoff, helps maintain soil moisture and provides microsites for vegetation establishment.

Substantial vegetation regrowth was measured 10 years post fire across all fires and burn severities. Understorey GV, NPV and inorganic cover proportions were nearly equal on all sites 10 years post fire regardless of whether they were initially classified as low, moderate or high burn severity. The convergence of cover fractions between burn severity classes after 10 years may constitute the single best indicator of post-fire recovery. The shift in associations from char (immediately post fire) to understorey GV and litter (10 years post fire) occurred at varying rates depending on the initial degree of disturbance, and represents a continuum of responses that we were able to infer from the initial post-fire HS images and confirm from the 2007 QB and 2007 and 2013 Landsat images. The proportional cover combinations of char and soil, understorey GV and NPV capture the dynamics of burn severity and vegetation recovery. This study adds to the growing evidence that scalable fractional cover components have a firmer biophysical basis than field (e.g. Composite Burn Index, CBI) or remotely sensed (e.g. dNBR) burn severity indices with less interpretability (Roy *et al.* 2006).

Conflicts of interest

The authors declare that they have no conflicts of interest.

Acknowledgements

This research was supported in part by funds provided by the Rocky Mountain Research Station, Forest Service, USDA, to the University of Idaho (USDA/USDI Joint Fire Science Program grants JFSP 03–2-1–02 and 14–1-02–27, via Research Joint Venture Agreements 03-JV-111222065–279 and 14-JV-11221633–112 respectively), NASA under award NNX11AO24G, and the University of Idaho. J. Hedgecock, S. Jenkins, S. MacDonald, K. C. Murdock, B. Parker, J. Sandquist, D. Shipton and C. Stone assisted with field data collection in 2003 and 2004, and J. Young and C. Kvamme with initial data entry. J. Byrne, J. Trujillo, J. Rigg, R. Wagner and M. Shelton assisted on the 2013 field crew. The GIS work was facilitated by an *Arc Macro Language* (AML) routine written by J. Evans and executed by M. Bobbitt; S. Larson helped with figure preparation. We appreciate the help of local natural resources managers in each location for access to wildfires, as well as the incident management teams for their cooperation and willingness to provide access and information.

References

Abella SR, Fornwalt PJ (2015) Ten years of vegetation assembly after a North American mega fire. *Global Change Biology* **21**, 789–802. doi:10.1111/GCB.12722

Agee JK (1998) The landscape ecology of western fire regimes. *Northwest Science* **72**, 24–34.

AIG (Analytical Imaging and Geophysics, LLC) (2002) 'ACORN 5.0 User's Guide.' (AIG: Boulder, CO, USA)

Arno SF, Parsons DJ, Keane RE (2000) Mixed-severity fire regimes in the Northern Rocky Mountains: consequences of fire exclusion and options for the future. In 'Proceedings of the wilderness science in a time of change conference, Vol. 5: Wilderness ecosystems, threats and management'. (Eds DN Cole, SF McCool, WT Borrie, J O'Laughlin) USDA Forest Service, Rocky Mountain Research Station, Proceedings RMRS-P-15-VOL-5, pp. 225–232. (Fort Collins, CO, USA)

ASD (Analytical Spectral Devices, Inc.) (2002) 'FieldSpec Pro User's Guide.'(ASD: Boulder, CO, USA)

Bartels SF, Chen HYH, Wulder MA, White JC (2016) Trends in post-disturbance recovery rates of Canada's forests following wildfire and harvest. *Forest Ecology and Management* **361**, 194–207. doi:10.1016/J.FORECO.2015.11.015

Bataineh AL, Oswald BP, Bataineh MM, Williams HM, Coble DW (2006) Changes in understory vegetation of a ponderosa pine forest in northern Arizona 30 years after a wildfire. *Forest Ecology and Management* **235**, 283–294. doi:10.1016/J.FORECO.2006.09.003

Berryman EM, Morgan P, Robichaud PR, Page-Dumroese D (2014) Post-fire erosion control mulches alter belowground processes and nitrate reductase activity of a perennial forb, heartleaf arnica (*Arnica cordifolia*). USDA Forest Service, Rocky Mountain Research Station, Research Note RMRS-RN-69. (Fort Collins, CO, USA)

Bowman DMJ, Balch JK, Artaxo P, Bond WJ, Carlson JM, Cochrane MA, D'Antonio CM, DeFries RS, Doyle JC, Harrison SP, Johnston FH, Keeley JE, Krawchuk MA, Kull CA, Marston JB, Moritz MA, Prentice IC, Roos CI, Scott AC, Swetnam TW, van der Werf GR, Pyne SJ (2009) Fire in the Earth system. *Science* **324**, 481–484. doi:10.1126/SCIENCE.1163886

Clark RN, Swayze GA, Livo KE, Kokaly RF, King TV, Dalton JB, Vance JS, Rockwell BW, Hoefen T, McDougal RR (2002) Surface reflectance calibration of terrestrial imaging spectroscopy data: a tutorial using AVIRIS. In 'Proceedings of the 10th JPL airborne sciences workshop (Pasadena, CA, 27 February–2 March 2001'. (Ed. RO Green) (Jet Propulsion Laboratory: Pasadena, CA) Available at http://speclab.cr.usgs.gov/PAPERS.calibration.tutorial [Accessed 23 November 2016]

Cochrane MA, Souza CM (1998) Linear mixture model classification of burned forests in the eastern Amazon. *International Journal of Remote Sensing* **19**, 3433–3440. doi:10.1080/014311698214109

Cocke AE, Fule PZ, Crouse JE (2005) Comparison of burn severity assessments using Differenced Normalized Burn Ratio and ground data. *International Journal of Wildland Fire* **14**, 189–198. doi:10.1071/WF04010

Cooper SV, Neiman KE, Roberts DW (1991) Forest habitat types of northern Idaho: a second approximation. USDA Forest Service, Intermountain Research Station, General Technical Report INT-236. (Ogden, UT, USA)

Dale VH, Joyce LA, McNulty S, Neilson RP, Ayres MP, Flannigan MD, Hanson PJ, Irland LC, Lugo AE, Peterson CJ, Simberloff D, Swanson FJ, Stocks BJ, Wotton BM (2001) Climate change and forest disturbances: climate change can affect forests by altering the frequency, intensity, duration, and timing of fire, drought, introduced species, insect and pathogen outbreaks, hurricanes, windstorms, ice storms, or landslides. *Bioscience* **51**(9), 723–734. doi:10.1641/0006-3568(2001)051[0723:CCAFD]2.0.CO;2

Dennison PE, Roberts DA (2003) Endmember selection for multiple endmember spectral mixture analysis using endmember average RMSE. *Remote Sensing of Environment* **87**, 123–135. doi:10.1016/S0034-4257(03)00135-4

Dennison PE, Halligan KQ, Roberts DA (2004) A comparison of error metrics and constraints for multiple endmember spectral mixture analysis and spectral angle mapper. *Remote Sensing of Environment* **93**, 359–367. doi:10.1016/J.RSE.2004.07.013

Diaz-Delgado R, Lloret F, Pons X (2003) Influence of fire severity on plant regeneration by means of remote sensing imagery. *International Journal of Remote Sensing* **24**, 1751–1763. doi:10.1080/01431160210144732

Eckmann TC, Roberts DA, Still CJ (2008) Using multiple endmember spectral mixture analysis to retrieve subpixel fire properties from MODIS. *Remote Sensing of Environment* **112**, 3773–3783. doi:10.1016/J.RSE.2008.05.008

Eidenshink J, Schwind B, Brewer K, Zhu ZL, Quayle B, Howard S (2007) A project for monitoring trends in burn severity. *Fire Ecology* **3**, 3–21. doi:10.4996/FIREECOLOGY.0301003

Fernandez-Manso A, Quintano C, Roberts DA (2016) Burn severity influence on post-fire vegetation cover resilience from Landsat MESMA fraction images time series in Mediterranean forest ecosystems. *Remote Sensing of Environment* **184**, 112–123. doi:10.1016/J.RSE.2016.06.015

Fischer WC, Bradley AF (1987) Fire ecology of western Montana forest habitat types. USDA Forest Service, Intermountain Research Station, General Technical Report INT-223. (Ogden, UT, USA)

French NHF, Goovaerts P, Kasischke ES (2004) Uncertainty in estimating carbon emissions from boreal forest fires. *Journal of Geophysical Research* **109**, D14S08. doi:10.1029/2003JD003635

Hayes JJ, Robeson SM (2011) Relationships between fire severity and post-fire landscape pattern following a large mixed-severity fire in the Valle Vidal, New Mexico, USA. *Forest Ecology and Management* **261**, 1392–1400. doi:10.1016/J.FORECO.2011.01.023

Hicke JA, Asner GP, Kasischke ES, French NHF, Randerson JT, Collatz GJ, Stocks BJ, Tucker CJ, Los SO, Field CB (2003) Post-fire response of North American boreal forest net primary productivity analyzed with satellite observations. *Global Change Biology* **9**, 1145–1157. doi:10.1046/J.1365-2486.2003.00658.X

Holden ZA, Morgan P, Smith AMS, Vierling L (2010) Beyond Landsat: a comparison of four satellite sensors for detecting burn severity in ponderosa pine forests of the Gila Wilderness, NM, USA. *International Journal of Wildland Fire* **19**, 449–458. doi:10.1071/WF07106

Hudak AT, Morgan P, Bobbitt M, Smith AMS, Lewis SA, Lentile LB (2007) The relationship of multispectral satellite imagery to immediate fire effects. *Fire Ecology* **3**, 64–90. doi:10.4996/FIREECOLOGY.0301064

Hudak AT, Ottmar RD, Vihnanek RE, Brewer NW, Smith AMS, Morgan P (2013) The relationship of post-fire white ash cover to surface fuel consumption. *International Journal of Wildland Fire* **22**, 780–785. doi:10.1071/WF12150

Idris MH, Kurajo K, Suzuki M (2005) Evaluating vegetation recovery following large-scale forest fires in Borneo and north-eastern China using multitemporal NOAA-AVHRR images. *Journal of Forest Research* **10**, 101–111. doi:10.1007/S10310-004-0106-Y

Kashian DM, Romme WH, Tinker DB, Turner MG, Ryan MG (2006) Carbon storage on landscapes with stand-replacing fires. *Bioscience* **56**, 598–606. doi:10.1641/0006-3568(2006)56[598:CSOLWS]2.0.CO;2

Kokaly RF, Rockwell BW, Haire SL, King TVV (2007) Characterization of post-fire surface cover, soils, and burn severity and the Cerro Grande Fire, New Mexico, using hyperspectral and multispectral remote sensing. *Remote Sensing of Environment* **106**, 305–325. doi:10.1016/J.RSE.2006.08.006

Kolden CA, Lutz LA, Key CH, Kane JT, van Wagtendonk JW (2012) Mapped versus actual burned area within wildfire perimeters: characterizing the unburned *Forest Ecology and Management* **286**, 38–47. doi:10.1016/J.FORECO.2012.08.020

Kolden CA, Smith AMS, Abatzoglou JT (2015) Limitations and utilisation of Monitoring Trends in Burn Severity products for assessing wildfire severity in the USA. *International Journal of Wildland Fire* **24**, 1023–1028.

Lentile LB, Holden ZA, Smith AMS, Falkowski MJ, Hudak AT, Morgan P, Lewis SA, Gessler PE, Benson NC (2006) Remote sensing techniques to assess active fire characteristics and post-fire effects. *International Journal of Wildland Fire* **15**, 319–345. doi:10.1071/WF05097

Lentile LB, Morgan P, Hudak AT, Bobbitt MJ, Lewis SA, Smith AMS, Robichaud PR (2007*a*) Burn severity and vegetation response following eight large wildfires across the western US. *Fire Ecology* **3**, 91–108. doi:10.4996/FIREECOLOGY.0301091

Lentile L, Morgan P, Hardy C, Hudak A, Means R, Ottmar R, Robichaud P, Sutherland E, Way F, Lewis S (2007*b*) Lessons learned from rapid response research on wildland fires. *Fire Management Today* **67**(1), 24–31.

Lentile LB, Smith AMS, Hudak AT, Morgan P, Bobbitt MJ, Lewis SA, Robichaud PR (2009) Remote sensing for prediction of 1-year post-fire ecosystem condition. *International Journal of Wildland Fire* **18**, 594–608. doi:10.1071/WF07091

Lewis SA, Lentile LB, Hudak AT, Robichaud PR, Morgan P, Bobbitt MJ (2007) Mapping ground cover using hyperspectral remote sensing after the 2003 Simi and Old wildfires in southern California. *Fire Ecology* **3**, 109–128. doi:10.4996/FIREECOLOGY.0301109

Lewis SA, Hudak AT, Ottmar RD, Robichaud PR, Lentile LB, Hood SM, Cronan JB, Morgan P (2011) Using hyperspectral imagery to estimate forest floor consumption from wildfire in boreal forests of Alaska, USA. *International Journal of Wildland Fire* **20**, 255–271. doi:10.1071/WF09081

Li L, Ustin SL, Lay M (2005) Application of multiple endmember spectral mixture analysis (MESMA) to AVIRIS imagery for coastal salt marsh mapping: a case study in China Camp, CA, USA. *International Journal of Remote Sensing* **26**, 5193–5207. doi:10.1080/01431160500218911

Loehman RA, Reinhardt E, Riley KL (2014) Wildland fire emissions, carbon, and climate: seeing the forest and the trees – a cross-scale assessment of wildfire and carbon dynamics in fire-prone, forested ecosystems. *Forest Ecology and Management* **317**, 9–19. doi:10.1016/J.FORECO.2013.04.014

Morgan P, Keane RE, Dillon GK, Jain TB, Hudak AT, Karau EC, Sikkink PG, Holden ZA, Strand EK (2014) Challenge of assessing fire and burn severity using field measures, remote sensing and modelling. *International Journal of Wildland Fire* **23**, 1045–1060. doi:10.1071/WF13058

Neary DG, Klopatek CC, DeBano LF, Ffolliott PF (1999) Fire effects on belowground sustainability: a review and synthesis. *Forest Ecology and Management* **122**, 51–71. doi:10.1016/S0378-1127(99)00032-8

Okin GS, Roberts DA, Murray B, Okin WJ (2001) Practical limits on hyperspectral vegetation discrimination in arid and semiarid environments. *Remote Sensing of Environment* **77**, 212–225. doi:10.1016/S0034-4257(01)00207-3

Page-Dumroese DS, Abbott AM, Rice TM (2009) Forest soil disturbance mapping protocol. Volume II: Supplementary methods, statistics, and data collection. USDA Forest Service, General Technical Report WO-82b. (Washington, DC, USA)

Parsons A, Robichaud PR, Lewis SA, Napper C, Clark JT (2010) Field guide for mapping post-fire soil burn severity. USDA Forest Service, Rocky Mountain Research Station, General Technical Report RMRS-GTR-243. (Fort Collins, CO, USA)

Perry DA, Hessburg PF, Skinner CN, Spies TA, Stephens SL, Taylor AH, Franklin JF, McComb B, Riegel G (2011) The ecology of mixed severity fire regimes in Washington, Oregon, and northern California. *Forest Ecology and Management* **262**, 703–717. doi:10.1016/J.FORECO.2011.05.004

Peters DP, Pielke RA, Bestelmeyer BT, Allen CD, Munson-McGee S, Havstad KM (2004) Cross-scale interactions, non-linearities, and forecasting catastrophic events. *Proceedings of the National Academy of Sciences of the United States of America* **101**, 15130–15135. doi:10.1073/PNAS.0403822101

Pfister RD, Kovalchik BL, Arno SF, Presby RC (1977) Forest habitat types of Montana. USDA Forest Service, Intermountain Research Station, General Technical Report INT-34. (Ogden, UT, USA)

Powell RL, Roberts DA (2008) Characterizing variability of the urban physical environment for a suite of cities in Rondonia, Brazil. *Earth Interactions* **12**, 1–32. doi:10.1175/2008EI246.1

Quintano C, Fernandez-Manso A, Roberts DA (2013) Multiple Endmember Spectral Mixture Analysis (MESMA) to map burn severity levels from Landsat images in Mediterranean countries. *Remote Sensing of Environment* **136**, 76–88. doi:10.1016/J.RSE.2013.04.017

Quintano C, Fernandez-Manso A, Roberts DA (2017) Burn severity mapping from Landsat MESMA fraction images and land surface temperature. *Remote Sensing of Environment* **190**, 83–95. doi:10.1016/J.RSE.2016.12.009

Richards JA, Jia X (1999) 'Remote sensing digital image analysis: an introduction', 3rd edn. (Springer Verlag: Berlin, Germany)

Roberts DA, Smith MO, Adams JB (1993) Green vegetation, nonphotosynthetic vegetation, and soils in AVIRIS data. *Remote Sensing of Environment* **44**, 255–269. doi:10.1016/0034-4257(93)90020-X

Roberts DA, Gardner M, Church R, Ustin S, Scheer G, Green RO (1998) Mapping chaparral in the Santa Monica Mountains using multiple endmember spectral mixture models. *Remote Sensing of Environment* **65**, 267–279. doi:10.1016/S0034-4257(98)00037-6

Robichaud PR, Lewis SA, Laes DYM, Hudak AT, Kokaly RF, Zamudio JA (2007) Post-fire soil burn severity mapping with hyperspectral image unmixing. *Remote Sensing of Environment* **108**, 467–480. doi:10.1016/J.RSE.2006.11.027

Rocca ME, Miniat CF, Mitchell RJ (2014) Introduction to the regional assessments: climate change, wildfire, and forest ecosystem services in the USA. *Forest Ecology and Management* **327**, 265–268. doi:10.1016/J.FORECO.2014.06.007

Rogan J, Yool SR (2001) Mapping fire-induced vegetation depletion in the Peloncillo Mountains, Arizona and New Mexico. *International Journal of Remote Sensing* **22**, 3101–3121. doi:10.1080/01431160152558279

Romme WH, Boyce MS, Gresswell R, Merrill EH, Minshall GW, Whitlock C, Turner MG (2011) Twenty years after the 1988 Yellowstone fires: lessons about disturbance and ecosystems. *Ecosystems* **14**, 1196–1215. doi:10.1007/S10021-011-9470-6

Roth KL, Dennison PE, Roberts DA (2012) Comparing endmember selection techniques for accurate mapping of plant species and land cover using imaging spectrometer data. *Remote Sensing of Environment* **127**, 139–152. doi:10.1016/J.RSE.2012.08.030

Roy DP, Boschetti L, Trigg SN (2006) Remote sensing of fire severity: assessing the performance of the Normalized Burn Ratio. *IEEE Geoscience and Remote Sensing Letters* **3**, 112–116. doi:10.1109/LGRS.2005.858485

RSAC (Remote Sensing Applications Center) (2005) Remote Sensing Applications Center Burned Area Emergency Response (BAER) imagery support. USDA Forest Service, Remote Sensing Applications Center. (Salt Lake City, UT, USA) Available at http://www.fs.fed.us/eng/rsac/baer/ [Accessed 10 June 2016]

Ryan KC (2002) Dynamic interactions between forest structure and fire behavior in boreal ecosystems. *Silva Fennica* **36**, 13–39. doi:10.14214/SF.548

Sá ACL, Pereira JMC, Vasconcelos MJP, Silva JMN, Ribeiro N, Awasse A (2003) Assessing the feasibility of subpixel burned area mapping in miombo woodlands of northern Mozambique using MODIS imagery. *International Journal of Remote Sensing* **24**, 1783–1796. doi:10.1080/01431160210144750

Sankey JB, Wallace CSA, Ravi S (2013) Phenology-based, remote sensing of post-burn disturbance windows in rangelands. *Ecological Indicators* **30**, 35–44. doi:10.1016/J.ECOLIND.2013.02.004

SAS Institute Inc. (2003) 'SAS System software.' (SAS Institute Inc.: Cary, NC, USA)

Schoennagel T, Smithwick EAH, Turner MG (2008) Landscape heterogeneity following large fires: insights from Yellowstone National Park, USA. *International Journal of Wildland Fire* **17**, 742–753. doi:10.1071/WF07146

Settle JJ, Drake NA (1993) Linear mixing and the estimation of ground cover proportions. *International Journal of Remote Sensing* **14**, 1159–1177. doi:10.1080/01431169308904402

Shive KL, Sieg CH, Fulé PZ (2013) Pre-wildfire management treatments interact with fire severity to have lasting effects on post-wildfire vegetation response. *Forest Ecology and Management* **297**, 75–83. doi:10.1016/J.FORECO.2013.02.021

Smith AMS, Hudak AT (2005) Estimating combustion of large downed woody debris from residual white ash. *International Journal of Wildland Fire* **14**, 245–248. doi:10.1071/WF05011

Smith AMS, Wooster MJ, Drake NA, Dipotso FM, Falkowski MJ, Hudak AT (2005) Testing the potential of multispectral remote sensing for retrospectively estimating fire severity in African savannahs environments. *Remote Sensing of Environment* **97**, 92–115. doi:10.1016/J.RSE.2005.04.014

Smith AMS, Lentile LB, Hudak AT, Morgan P (2007*a*) Evaluation of linear spectral unmixing and dNBR for predicting post-fire recovery in a North American ponderosa pine forest. *International Journal of Remote Sensing* **28**, 5159–5166. doi:10.1080/01431160701395161

Smith AMS, Drake NA, Wooster MJ, Hudak AT, Holden ZA, Gibbons CJ (2007*b*) Production of Landsat ETM+ reference imagery of burned areas within southern African savannas: comparison of methods and application to MODIS. *International Journal of Remote Sensing* **28**, 2753–2775. doi:10.1080/01431160600954704

Smith AMS, Eitel JUH, Hudak AT (2010) Spectral analysis of charcoal on soils: implications for wildland fire severity mapping methods. *International Journal of Wildland Fire* **19**, 976–983. doi:10.1071/WF09057

Smith AMS, Kolden CA, Tinkham WT, Talhelm A, Marshall JD, Hudak AT, Boschetti L, Falkowski MJ, Greenberg JA, Anderson JW, Kliskey A, Alessa L, Keefe RF, Gosz J (2014) Remote sensing the vulnerability of

vegetation in natural terrestrial ecosystems. *Remote Sensing of Environment* **154**, 322–337. doi:10.1016/J.RSE.2014.03.038

Smith AMS, Sparks AM, Kolden CA, Abatzoglou JT, Talhelm AF, Johnson DM, Boschetti L, Lutz JA, Apostol KG, Yedinak KM, Tinkham WT, Kremens RJ (2016) Towards a new paradigm in fire severity research using dose–response experiments. *International Journal of Wildland Fire* **25**, 158–166. doi:10.1071/WF15130

Stephan K, Kavanagh KL, Koyama A (2012) Effects of spring prescribed burning and wildfires on watershed nitrogen dynamics of central Idaho headwater areas. *Forest Ecology and Management* **263**, 240–252. doi:10.1016/J.FORECO.2011.09.013

Tompkins S, Mustard JF, Pieters CM, Forsyth DW (1997) Optimization of endmembers for spectral mixture analysis. *Remote Sensing of Environment* **59**, 472–489. doi:10.1016/S0034-4257(96)00122-8

van Wagtendonk JW, Root RR, Key CH (2004) Comparison of AVIRIS and Landsat ETM+ detection capabilities for burn severity. *Remote Sensing of Environment* **92**, 397–408. doi:10.1016/J.RSE.2003.12.015

Veraverbeke S, Hook SJ (2013) Evaluating spectral indices and spectral mixture analysis for assessing fire severity, combustion completeness, and carbon emissions. *International Journal of Wildland Fire* **22**, 707–720. doi:10.1071/WF12168

Veraverbeke S, Hook SJ, Harris S (2012) Synergy of VSWIR (0.4–2.5 μm) and MTIR (3.5–12.5 μm) data for post-fire assessments. *Remote Sensing of Environment* **124**, 771–779. doi:10.1016/J.RSE.2012.06.028

Viedma O, Meliá J, Segarra D, Garcia-Haro J (1997) Modeling rates of ecosystem recovery after fires by using Landsat TM data. *Remote Sensing of Environment* **61**, 383–398. doi:10.1016/S0034-4257(97)00048-5

Viedma O, Torres I, Perez B, Moreno JM (2012) Modeling plant species richness using reflectance and texture data derived from QuickBird in a recently burned area of central Spain. *Remote Sensing of Environment* **119**, 208–221. doi:10.1016/J.RSE.2011.12.024

Wang JJ, Zhang Y, Bussink C (2012) Unsupervised multiple endmember spectral mixture analysis-based detection of opium poppy fields from an EO-1 Hyperion image in Helmand, Afghanistan. *The Science of the Total Environment* **476–477**, 1–6.

Willis KS (2015) Remote sensing change detection for ecological monitoring in United States protected areas. *Biological Conservation* **182**, 233–242. doi:10.1016/J.BIOCON.2014.12.006

Wittenberg L, Malkinson D, Beeri O, Halutzy A, Tesler N (2007) Spatial and temporal patterns of vegetation recovery following sequences of forest fires in a Mediterranean landscape, Mt Carmel, Israel. *Catena* **71**, 76–83. doi:10.1016/J.CATENA.2006.10.007

Yang J, He Y, Caspersen J (2015) Fully constrained linear spectral unmixing-based global shadow compensation for high-resolution satellite imagery of urban areas. *International Journal of Applied Earth Observation and Geoinformation* **38**, 88–98. doi:10.1016/J.JAG.2014.12.005

Youngentob KN, Roberts DA, Held AA, Dennison PE, Jia X, Lindenmayer DB (2011) Mapping two *Eucalyptus* subgenera using multiple endmember spectral mixture analysis and continuum-removed imaging spectrometry data. *Remote Sensing of Environment* **115**, 1115–1128. doi:10.1016/J.RSE.2010.12.012